Reactions of Ar$^+$ with Selected Volatile Organic Compounds. A Flowing Afterglow and Selected Ion Flow Tube Study

Michael H. Cohen, Cynthia Barckholtz, Brian T. Frink, Joshua J. Bond, C. Michael Geise, Jerry Hoff, John Herlinger, Tom Hickey, and Christopher M. Hadad*

Department of Chemistry, The Ohio State University, 100 West 18th Avenue, Columbus, Ohio 43210-1173

Temperature-dependent rate coefficients and branching ratios for the reactions of Ar$^+$ with a variety of volatile organic hydrocarbons are reported. Reactions of N$_2^+$ and CO$_2^+$ were undertaken to calibrate a newly constructed variable-temperature flowing afterglow (VTFA) complemented with a selected ion flow tube (SIFT). In addition, the first determinations of rate coefficients for the reaction of Ar$^+$ with several organic hydrocarbons (toluene, pyridine, furan, thiophene, cyclohexene, cyclooctene, cyclohexane, and tetrahydrofuran) have been measured between 298 and 423 K with a VT-SIFT. Analogous to the Ar$^+$ + C$_6$H$_6$ reaction, these reactions proceed by nondissociative and dissociative charge transfer, and very little temperature dependence is observed for the rate coefficients. At 298 K and 0.5 Torr, the rate coefficients are similar [(1.4−1.8) × 10^{-9} cm^3/s] for all of the Ar$^+$ reactions with the organic hydrocarbons, except for pyridine (2.3 × 10^{-9} cm^3/s). These values are in reasonable agreement with rate coefficients predicted from average dipole orientation (ADO) theory. The degree of fragmentation appears to be loosely correlated to the difference in ionization potential between Ar$^+$ and that of the neutral compounds as well as the degree of unsaturation of the hydrocarbon.

I. Introduction

The study of gas-phase ion−molecule reactions has made significant contributions to many areas of chemistry, including combustion, plasma, and ionospheric chemistry.[1,2] One of the most commonly observed processes in gas-phase ion chemistry is charge transfer, in which a single electron is transferred from the neutral reagent to the reactant cation. Charge-transfer reactions have been studied by a variety of methods, including ion beam techniques[3,4] and mass spectrometric techniques.[5,6]

The flowing afterglow (FA) technique, introduced by Ferguson, Fehsenfeld, and Schmeltekopf in 1963, is now an established method for studying the reaction kinetics of ion−molecule reactions.[7] Initially, the FA contributed tremendously in the determination of quantitative rate coefficients for ion−molecule reactions of ionospheric and atmospheric interest. Although the FA method is very useful in the study of ion−molecule reactions under well-characterized conditions and temperatures, the technique is limited by the ability to generate the desired ion synthetically without the presence of any other ions. Furthermore, the ions are generated in a plasma that will contain positive ions, negative ions, and electrons, and these species may complicate the observed chemistry. As a result, there may be ambiguity in the identification of primary products from a specific reactant as well as the partial inability to distinguish between the desired reaction and other competitive processes.

Smith and Adams realized that some of these problems could be resolved if the desired ion could be mass selected ("purified") from an ion plasma generated in a remote source, and their efforts led to the development of the selected ion flow tube (SIFT).[8] The greatest challenge to its implementation was how to efficiently introduce the ions from the low-pressure, mass-selection region (typically 10^{-5} Torr) into the high-pressure reaction region (typically 0.5 Torr). This problem was first solved by the use of an injector flange that introduced the helium carrier gas through an inlet at the point of ion injection in such a manner that the pressure was reduced in the ion injection region.[9] The NOAA laboratory[10] demonstrated the benefit of a venturi inlet over the initial hole-pattern design, and the venturi design was exploited successfully by DePuy, Bierbaum, and co-workers.[11] Since then, the widely recognized advantages of the SIFT have led to the adoption of the technique in several laboratories,[11−18] and several detailed descriptions of the SIFT technique have been reported.[9,19,20] Recently, Fishman and Grabowski have reported a flexible hole-pattern design and demonstrated its utility for some positive ion reactions.[14]

The most common design for current FA-SIFT instruments is a linear geometry,[11] and as a result, the mass-selection chamber is on-axis with the ion source. One of the greatest limitations for quadrupole resolution is the presence of background gas in the quadrupole chamber. This effect can be minimized if the ion beam can be separated from the carrier gas introduced in the flowing afterglow source. A novel design[21] for our FA-SIFT was chosen in an effort to reduce the effect that the neutral gas load would have on the sensitivity of the selection quadrupole. In the design presented here, an electrostatic quadrupole deflector (QD) is introduced into the ion path immediately before the mass-selection quadrupole. The QD thereby filters the ions away from the neutrals which have passed through the initial skimmer (nose cone orifice).

The QD has long been used as a focusing device, but was first described in theory and applied in practice to merge oppositely charged ion beams by Zeman.[22] Since then, the

---

Reactions of Ar$^+$ with Volatile Organic Compounds

J. Phys. Chem. A, Vol. 104, No. 48, 2000 **11319**

Variable Temperature Flowing Afterglow - Selected Ion Flow Tube with a Neutral Flow Reactor
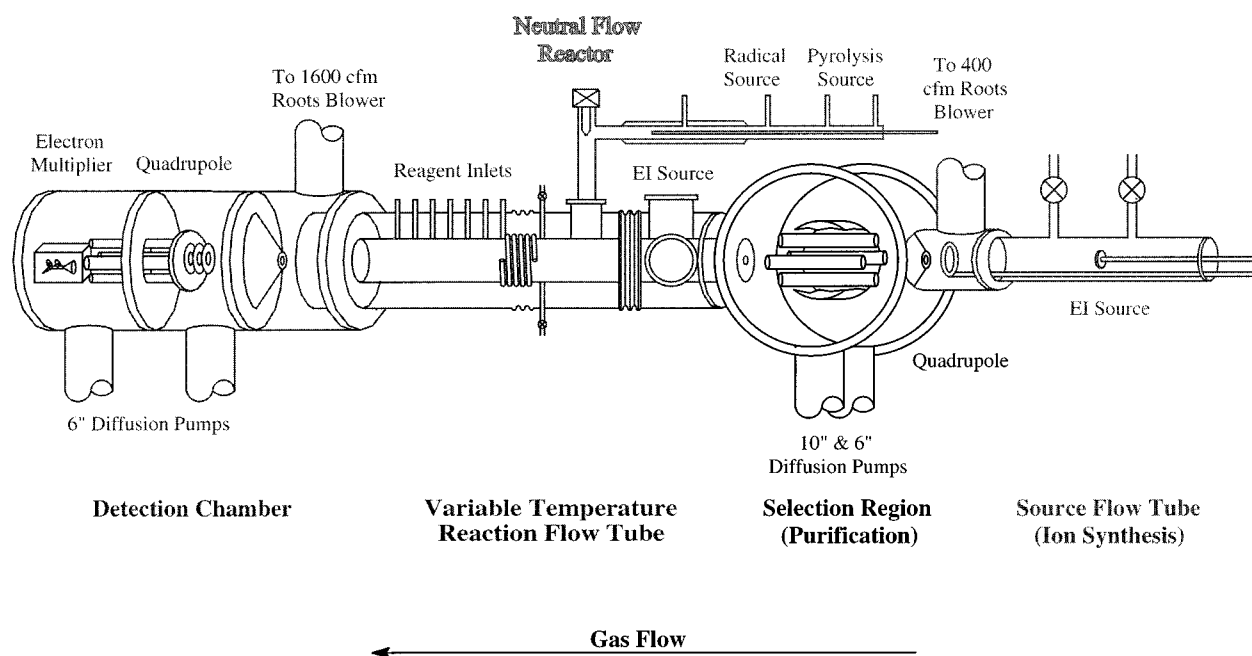
Figure 1. General diagram of our variable-temperature flowing afterglow selected ion flow tube (VTFA-SIFT) with a neutral flow reactor.

quadrupole deflector has also been used to obtain the coaxial overlap of an ion and a laser beam,[23,24] to merge oppositely charged clustered ion beams,[25] and as a means to extract ions from different ion sources.[26] The Zeman QD employed shims and cylindrical electrodes to approximate the hyperbolic field of the theoretical quadrupole deflector. The deflector quadrupole designed for our SIFT chamber is similar to that of Posey and co-workers;[27] it was patterned after a simple design without shims originally described by Farley[23] and further characterized by Mahaffy and Lai.[26]

Recently, the role of charge transfer and ionization in hydrocarbon combustion has been explored.[28,29] Although many of the reactions that typically occur in combustion processes occur via neutral−neutral reactions, ion−molecule reactions are usually more facile as a result of the attractive potential of the ion. Recent results indicate that the inclusion of ionic mechanisms in combustion kinetic models increases the rate of combustion.[30] To this end, Viggiano and co-workers have studied a variety of ion−molecule reactions with several aliphatic[28,31] and a few aromatic hydrocarbons.[29,32]

With our current interest in combustion systems,[33−39] we have also begun to study the chemistry of ions derived from atmospheric constituents with a variety of organic substrates of relevance to fuels. As a preliminary step, in this paper, we report the nondissociative and dissociative charge-transfer reactions of Ar$^+$ with a series of organic hydrocarbons (benzene, toluene, pyridine, furan, thiophene, cyclohexene, cyclooctene, cyclohexane, and tetrahydrofuran). We present a brief summary of the design of the newly constructed VTFA-SIFT instrument that was used to study these reactions. Several well-established ion−molecule reactions involving atmospheric ions and VOCs were studied to demonstrate the working capability of our instrument. The first rate coefficients and product distributions

for the reaction of Ar$^+$ with a variety of aromatic hydrocarbons are then reported through the temperature range of 298−423 K.

II. Experimental Methods

Flowing Afterglow (FA). The FA method has been well described in the literature,[20] and only a brief description follows. A general diagram of the entire apparatus is presented in Figure 1.[40] One unique feature of our instrument is that the VTFA is complemented with a variable-temperature neutral flow reactor[41,42] and a SIFT. Ions in the FA are generated via electron ionization (EI) and traverse the length (∼1 m) of a stainless steel flow tube via a constant flow (typically 100 m/s) of a helium buffer gas.

The helium bath gas (Praxair, >99.995%) was purified by passing it through a copper coil, filled with 4 Å molecular sieves, which was immersed in a liquid nitrogen bath. The helium was preequilibrated to the desired temperature by flowing the gas through a 40 ft copper coil submerged in a constant-temperature bath, prior to entering the FA at the EI source. The effective temperature range of the VTFA is 77−533 K.

A blunt nose-cone skimmer (0.5 mm orifice) samples a small amount of the gas flow, which passes through two differentially pumped chambers (Edwards 6 in. diffusion pumps) via a set of electrostatic lenses and a 5/8 in. quadrupole (Extrel). Product ions are detected by an electron multiplier (DeTech) in pulse-counting mode. The detection system has unit mass resolution.

To determine reaction kinetics, seven (fixed) inlets in the ∼0.5 m reaction zone are available for the addition of neutral reagents to the ion flow. Most of the neutral reagents were purified by triplicate freeze−pump−thaw cycles. Rate coefficient studies were completed at a variety of temperatures and pressures, as noted below. The reaction rates were obtained under pseudo-
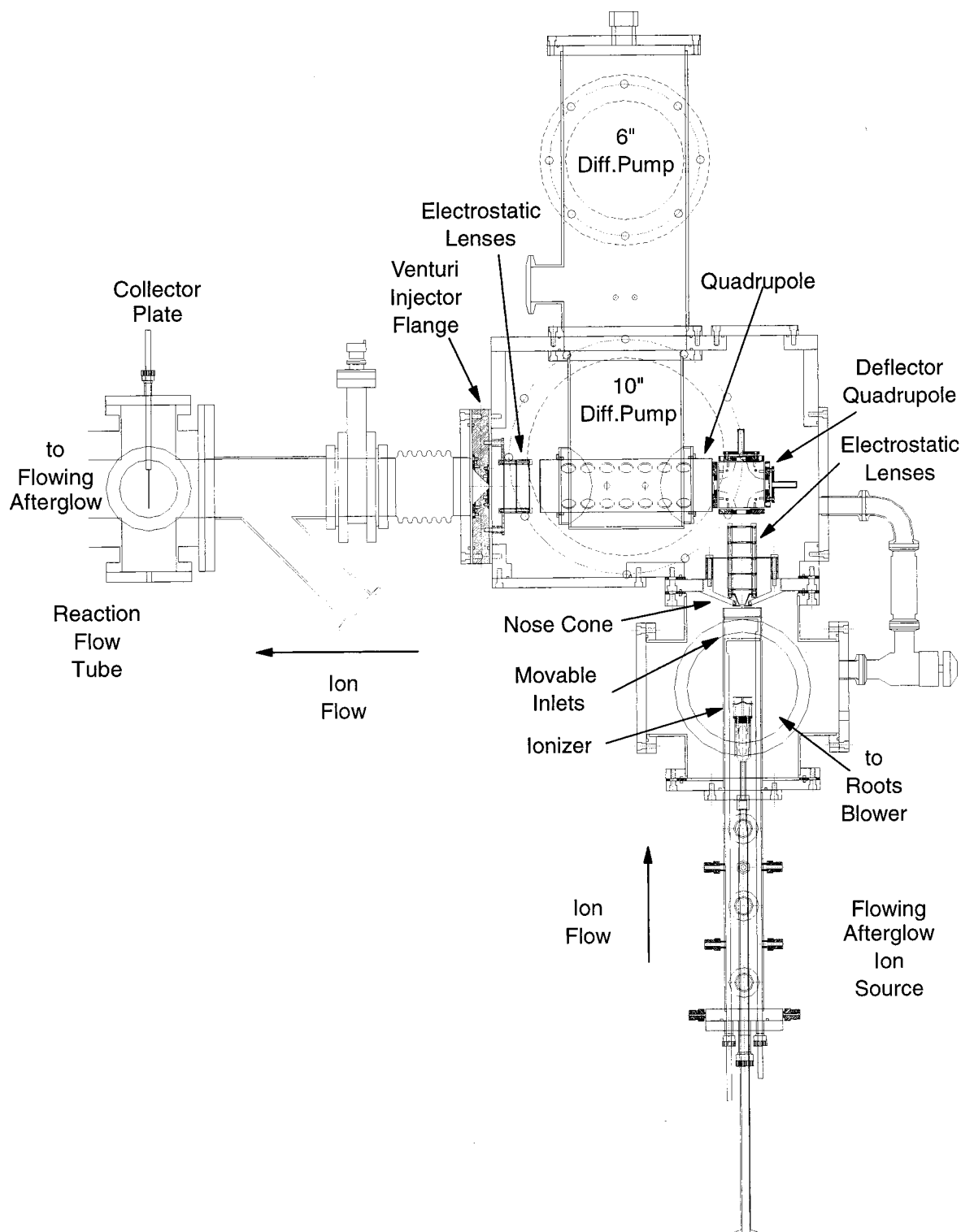
Figure 2. Detailed schematic diagram of the SIFT portion of the instrument which depicts the electrostatic quadrupole deflector (QD) which is used to bend the ions 90° into the mass-selection quadrupole.

first-order conditions with the neutral reagent in large excess. Primary product distributions, which are presented in the following tables, were obtained by extrapolating the normalized ion yields to the zero flow rate limit of the neutral reagent (except where noted below). Due to the extrapolation procedure, the product yields should be considered to have an absolute accuracy of ±10%.[43]

Selected Ion Flow Tube (SIFT). A schematic diagram of the SIFT chamber and its FA ion source is shown in Figure 2. A novel design for our FA-SIFT,[21] which incorporates a

quadrupole deflector (QD), was chosen in an effort to reduce the effect that the neutral gas load would have on the sensitivity of the mass selection quadrupole.

Ions in the FA source are generated by a precursor gas that is introduced via movable inlets into the flowing helium bath gas which then passes over an EI filament. A 400 cfm Roots blower (Stokes) exhausts most of the gas load introduced into the ion source region. A small portion of the gas flow is sampled into the low-pressure SIFT chamber through a blunt molybdenum orifice (3 mm).[7] The SIFT chamber is pumped by a 10 in.

TABLE 1: Variable Temperature Rate Coefficients (k) and Branching Ratios (%) for Calibration Reactions Obtained with the FA Technique[a]

reaction	298 K	323 K	348 K	373 K	398 K	423 K	lit. rate (298 K)[a,b]
$N_2^+ + O_2 \rightarrow$	$k = 1.18 \pm 0.38$	$k = 0.77 \pm 0.16$	$k = 0.88 \pm 0.16$	$k = 0.74 \pm 0.23$	$k = 0.63 \pm 0.20$	$k = 0.59 \pm 0.18$	$k = 0.50 \pm 0.08$
$O_2^+ + N_2$							
$N_2^+ + CO_2 \rightarrow$	$k = 10.0 \pm 5.2$						$k = 8.0 \pm 1.6$
$CO_2^+ + N_2$							
$CO_2^+ + O_2 \rightarrow$	$k = 1.14 \pm 0.43$	$k = 1.12 \pm 0.31$	$k = 0.96 \pm 0.22$	$k = 1.26 \pm 0.44$	$k = 1.06 \pm 0.30$	$k = 0.59 \pm 0.13$	$k = 0.55 \pm 0.08$
$O_2^+ + CO_2$							
$N_2^+ + CH_4 \rightarrow$	$k = 12.3 \pm 5.8$	$k = 6.5 \pm 0.5$	$k = 6.1 \pm 0.8$	$k = 8.7 \pm 1.4$	$k = 8.6 \pm 1.2$	$k = 9.7 \pm 1.7$	$k = 11.4 \pm 1.7$
$CH_2^+ + H_2 + N_2$	9	14	12	17	16	18	
$CH_3^+ + H + N_2$	77	81	83	80	81	79	
$CH_4^+ + N_2$	14	5	5	3	3	3	
$N_2^+ + CH_3OH \rightarrow$	$k = 14.1 \pm 2.9$	$k = 15.2 \pm 0.3$	$k = 16.2 \pm 0.6$	$k = 17.2 \pm 0.2$	$k = 17.6 \pm 0.1$	$k = 17.9 \pm 1.6$	$k = 14 \pm 4$
$CH_3^+ + OH + N_2$	53	63	63	63	63	61	
$CH_2OH^+ + H + N_2$	38	34	34	35	35	36	
$CH_3OH^+ + N_2$	9	3	3	2	2	3	
$N_2^+ + CS_2 \rightarrow$	$k = 10.2 \pm 3.8$						$k = 12 \pm 2$
$CS_2^+ + N_2$	45						
$S^+ + CS + N_2$	55						
$N_2^+ + CH_3CN \rightarrow$	$k = 16.8 \pm 1.3$						$k = 21 \pm 6$
$CH_3^+ + CN + N_2$	5						
$CH_2CN^+ + H + N_2$	43						
$CH_3CN^+ + N_2$	52						

[a] The rate coefficients are in units of 10^{-10} cm^3/s. [b] Anicich, V. G. *J. Phys. Chem. Ref. Data* **1994**, *22*, 1469.

diffusion pump (Edwards) that is backed by a 37 cfm rotary vane mechanical pump (Stokes). A typical pressure in the SIFT vacuum chamber is 1×10^{-6} Torr when the helium carrier gas is flowing in the source flow tube only.

Sampled ions are then focused by six electrostatic lenses within the SIFT chamber. An electrostatic quadrupole deflector[22,23,26,27] (QD) is introduced into the ion path immediately before the mass-selection quadrupole in order to bend the ions 90° into the SIFT chamber and away from the neutrals in the plasma. Use of two Faraday cups mounted on the exit lenses of the QD suggests that the ions are bent with >90% efficiency. Ions that are bent 90° by the QD are then focused into the ion selection 5/8 in. quadrupole (Extrel), which is differentially pumped by a 6 in. diffusion pump (Edwards) and backed by the same 37 cfm mechanical pump used for the 10 in. diffusion pump.

Mass-selected ions are then focused by 3 electrostatic lenses into a venturi injector, which injects ions from the low-pressure mass selection chamber into the high-pressure reaction flow tube. The design of our venturi injector is very similar to that of Van Doren et al.,[11] and is composed of inner and outer annuli with a 2 mm central aperture. Typically, about 40% of the helium flow enters through the inner annulus. As a result of back-streaming, the pressure in the mass-selection chamber is $\sim 1 \times 10^{-5}$ Torr with ~ 0.7 Torr in the reaction flow tube.

III. Experimental Calibration

The absolute rate coefficients reported here are accurate to within 25%. Unless otherwise noted, at least triplicate measurements were taken for all reactions studied; the errors are one standard deviation of the measurements reported to demonstrate the precision of the measurements. In the discussion and tables, we report the average rate coefficient of these multiple measurements, and the reported error represents one standard deviation.

A. FA Calibration Reactions. We have investigated the reactions of a few positive ions with a variety of neutral reagents for which rate coefficients have been studied[44] at room temperature, and a comparison of our values with the literature is presented in Table 1.

Non-Dissociative Charge-Transfer Reactions. The charge-transfer reaction of $N_2^+ + O_2 \rightarrow N_2 + O_2^+$ is important in atmospheric chemistry and has been well studied.[45−48] The rate coefficient for this reaction at 298 K has been determined many times, and reported values range from (0.50 ± 0.08) to 2.0×10^{-10} cm^3/s.[44,47] Our value of $(1.2 \pm 0.4) \times 10^{-10}$ cm^3/s falls within this range but is higher than the accepted value[44] of $(0.50 \pm 0.08) \times 10^{-10}$ cm^3/s. Our measurement of a faster rate is likely due to the presence of electrons in the FA plasma causing some loss of parent N_2^+ ion signal due to electron recombination. We have also studied the $N_2^+ + O_2 \rightarrow N_2 + O_2^+$ reaction in the temperature range of 298−423 K (Table 1), and have determined a temperature dependence of $T^{(-1.7\pm0.4)}$. Dunkin et al. [45] reported a temperature dependence of $T^{(-0.6)}$ from 300 to 600 K, while McFarland et al.[49] reported a temperature dependence of $T^{(-0.8\pm0.2)}$ for temperatures ≤ 3560 K. A negative temperature dependence is observed in the range of temperatures studied. The trend is similar to the prior experiments mentioned above; however, the magnitude of the dependence differs. This difference is likely due to electron recombination which occurs in the flow tube.

The charge-transfer reaction of $CO_2^+ + O_2$ has also been studied.[44,50,51] The rate coefficient at 298 K, 1.14×10^{-10} cm^3/s, is slightly higher than the accepted value (0.55×10^{-10} cm^3/s). A small negative temperature dependence is observed from 298 to 423 K; however, the uncertainty in the temperature dependence is large. Miller et al. have reported a negative temperature dependence over a wider temperature range (90−450 K).

Dissociative Charge-Transfer Reactions. The reactions of N_2^+ with CS_2, CH_3OH, CH_3CN, and CH_4 proceed by dissociative charge transfer (Table 1). In these cases, some fragmentation after charge transfer occurs and leads to the formation of S^+ and CS_2^+ (from carbon disulfide), $CHCN^+$, CH_2CN^+, and CH_3CN^+ (from acetonitrile), CH_3^+, CH_2OH^+, and CH_3OH^+ (from methanol), and CH_2^+ and CH_3^+ (from methane). In Table 1, the branching ratios are presented as relative yields of the

particular product ion (corresponding to the reaction channel indicated), normalized for the sum of all of the observed product ions. Our measured rate coefficient for the N_2^+ reaction with CS_2 is in excellent agreement with the literature. Although our measured rate for the reaction of N_2^+ with CH_3CN is slower than the reported value, there is a large uncertainty in the literature value.[44]

The rate coefficient at 298 K obtained for the reaction of N_2^+ with CH_3OH, $(14.1 \pm 2.9) \times 10^{-10}$ cm^3/s, is in excellent agreement with previously published results, $(14 \pm 4) \times 10^{-10}$ cm^3/s.[44] The reaction rate coefficient for N_2^+ with CH_3OH was found to have a slightly positive temperature dependence of $T^{(0.7 \pm 0.1)}$ in the range of 298 to 423 K. In agreement with previously published data,[44] the primary ionic product observed at all temperatures is CH_3^+, and the minor ionic products are CH_2OH^+ and CH_3OH^+.

Similarly, our FA measurement of the $N_2^+ + CH_4$ reaction rate coefficient, $(12.3 \pm 5.8) \times 10^{-10}$ cm^3/s, is also in good agreement with the accepted value, $(11.4 \pm 1.7) \times 10^{-10}$ cm^3/s, although the uncertainty in our measurement is rather large. We also found that the reaction of N_2^+ with methane has a positive temperature dependence of $T^{(1.7 \pm 0.5)}$ between the temperatures of 323 and 423 K. The major ionic product observed in the reaction of N_2^+ with CH_4 is CH_3^+ at all temperatures, which is in agreement with previous studies.[44] However, we also observe CH_4^+ as a minor product (<14%) in these experiments.

B. SIFT Calibration Reactions. Several reactions of atmospheric positive ions with neutrals were also studied using the FA-SIFT to ensure that no systematic errors are present in our instrument which includes a quadrupole deflector prior to the mass selection region. The most significant advantage of using a SIFT to study positive ion reactions is the absence of any negative ions and electrons in the reaction flow tube where the reaction kinetics are monitored.

However, one of the concerns in performing experiments with a SIFT is that during the injection of ions from the low-pressure mass selection chamber into the higher pressure reaction flow tube, the ions may not be thermalized.[10,11] Several experiments have been performed with O^+ reactions with N_2 in order to quantify the thermalization of the ions upon injection into the high-pressure FA. It has been well established that the ground state of O^+ reacts with N_2 to generate only NO^+, while electronically excited O^+ yields N_2^+ as well.[52] For our SIFT experiments of mass-selected O^+ with N_2, only NO^+ was observed. Thus, the injection of ions from our SIFT into the reaction flow tube proceeds in a sufficiently gentle manner.

Non-Dissociative Charge-Transfer Reactions. The rate coefficient for the room-temperature reaction of N_2^+ with O_2 was reexamined using the FA-SIFT. Whereas our FA measurement was approximately a factor of 2 larger than the accepted value of $(0.50 \pm 0.08) \times 10^{-10}$ cm^3/s,[44] our FA-SIFT measurement is in much better agreement $(0.76 \pm 0.06) \times 10^{-10}$ cm^3/s, consistent with electron recombination affecting the FA measurement. In addition, our SIFT rate coefficient is in better agreement with a previous SIFT value of 0.51×10^{-10} cm^3/s.[53] We also explored the pressure dependence of the $N_2^+ + O_2$ reaction in our SIFT, and the reaction rate is independent of pressure in the 0.5 to 0.7 Torr range.

The nondissociative charge-transfer reaction of N_2^+ with CO_2 was also reexamined using the FA-SIFT. Similar to the $N_2^+ + O_2$ reaction, a slower rate coefficient was also measured when using a mass-selected N_2^+ ion beam, and the agreement with the accepted value improved. Furthermore, the FA-SIFT method
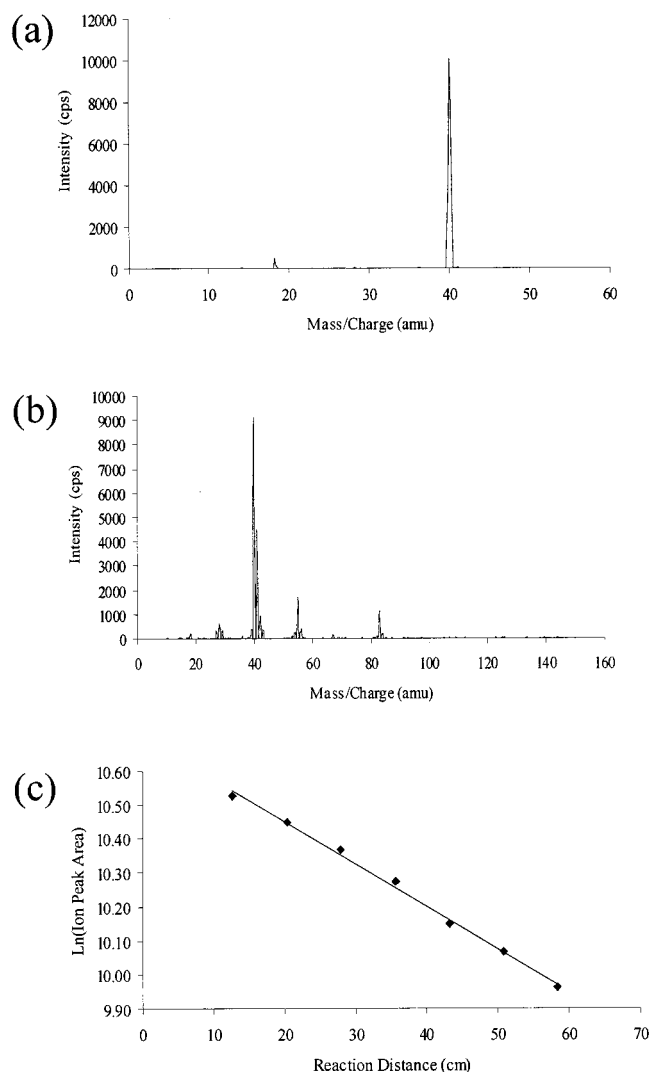
Figure 3. (a) A sample mass spectrum of "purified" Ar^+ as obtained with the SIFT. A small amount of H_2O^+ is present due to the presence of water in the helium flow of the reaction flow tube. (b) The mass spectrum that results from the reaction of Ar^+ with cyclohexane. (c) Semilogarithmic plot of integrated peak area for Ar^+ vs reaction distance (cm) to determine the bimolecular rate coefficient with cyclohexane.

provided a more precise measurement of the rate coefficient than did the FA method.

Dissociative Charge-Transfer Reactions. An improvement in the rate coefficient measurement for the reaction of mass-selected N_2^+ with CH_4 was also noted in the absence of the FA plasma. Furthermore, the (SIFT) product branching ratio observed in the reaction of N_2^+ with CH_4 is in good agreement with the literature.[44] The primary ionic product is CH_3^+, the minor ionic product is CH_2^+. In contrast to the FA experiment, no CH_4^+ is observed when this reaction is studied using a mass-selected beam of N_2^+.

IV. Results

The reactions of Ar^+ with a number of volatile organic compounds (VOCs) have been studied using the VTFA and SIFT in the temperature range of 298−423 K. Rate coefficients and branching ratios are presented for the reactions of Ar^+ with benzene, toluene, pyridine, furan, thiophene, cyclohexene, cyclooctene, cyclohexane, and tetrahydrofuran (THF). These compounds were chosen to represent some of the functional groups which may be present in fuels. A typical mass spectrum

Reactions of Ar$^+$ with Volatile Organic Compounds

J. Phys. Chem. A, Vol. 104, No. 48, 2000 **11323**

TABLE 2: Rate Coefficients and Branching Ratios (%) for Calibration Reactions Examined with the SIFT Technique at 298 K^a

reaction	P (Torr)	rate^a	lit. rate^{a,b}
$N_2^+ + O_2 \rightarrow O_2^+ + N_2$	0.5^c	0.76 ± 0.06	0.50 ± 0.08
	0.6	0.85 ± 0.12	
	0.7^c	0.81 ± 0.04	
$N_2^+ + CO_2 \rightarrow CO_2^+ + N_2$	0.6	9.3 ± 0.4	8.0 ± 1.6
$N_2^+ + CH_4 \rightarrow$	0.6	13.2 ± 0.9	11.4 ± 1.7
$CH_2^+ + H_2 + N_2$		21	
$CH_3^+ + H + N_2$		79	

^{a} The rate coefficients are in units of 10^{-10} cm^3/s. ^{b} Anicich, V. G. *J. Phys. Chem. Ref. Data* **1994**, *22*, 1469. ^{c} Only a single rate measurement was taken.

of mass-selected Ar$^+$ is shown in Figure 3a, and the ionic products of the Ar$^+$ + cyclohexane reaction (Figure 3b) are shown as an example of these dissociative charge-transfer reactions. A semilogarithmic kinetic plot (Figure 3c) is then used to determine the bimolecular rate coefficient.

Table 3 summarizes the results of SIFT measurements (298 K and 0.5 Torr) and FA measurements (0.5 Torr, $T = 298-423$ K) for these dissociative charge-transfer reactions. In addition, the calculated theoretical average dipole orientation (ADO)[54] rates are presented. It is evident from a comparison of our experimental rate coefficients with the values predicted by ADO theory that all of these charge-transfer reactions are very efficient.

In general, for the reactions studied here, very little change in rate coefficient is observed as a function of temperature. Experiments performed at 423 K in the FA at 0.5 Torr showed an increase in the bimolecular rate coefficient; however, this is likely due to nonlaminar helium flow. Experiments performed at 423 K and 1 Torr demonstrate that there is no significant temperature dependence.[55] Analogous data for SIFT measurements of the reaction of Ar$^+$ with benzene, toluene, and pyridine are presented in Table 4. These results indicate that within the accuracy of the experiments, the rate coefficients and product distributions are independent of both temperature and pressure.

Benzene. The Ar$^+$ + benzene reaction proceeds by dissociative charge transfer, and the dominant ionic products are $C_6H_6^+$, $C_6H_5^+$, $C_3H_3^+$, and $C_4H_n^+$ where $n = 2-5$. The observed product distribution is very similar for both the FA and SIFT studies. The rate coefficients measured with both FA and SIFT techniques are in good agreement with the recent study of Ar$^+$ (and other ions) with benzene by Viggiano and co-workers.[32] Within the range and accuracy of our experiments, the Ar$^+$ + benzene reaction is independent of temperature and pressure. This observation is consistent with the study of Viggiano and co-workers[32] over a similar temperature range.

Toluene. The reaction of Ar$^+$ with toluene occurs near to the collision rate, and significant fragmentation occurs. The dominant product ion peak is $C_7H_7^+$, and there is a small yield of the toluene radical cation. Also, fragmentation occurs to a greater extent at higher temperatures in the SIFT experiments, and $C_3H_3^+$ becomes a significant (~30%) product ion at 423 K. There is a slight increase in the rate coefficient for Ar$^+$ with toluene as a function of temperature in the small range examined here. The kinetic data obtained using both FA (Table 3) and SIFT techniques (Table 4) are in good agreement.

Pyridine. The reaction of Ar$^+$ with pyridine occurs at or near the ADO collision rate, and no temperature dependence is observed. The rate coefficient obtained with the SIFT at 0.5 Torr and 298 K is slightly higher than the ADO rate constant,

but still within the systematic precision of the experiment. Again, the FA and SIFT results are in good agreement.

The product ions that appear at m/z of 78 and 79 are clearly $C_5H_4N^+$ and $C_5H_5N^+$, respectively, and more fragmentation occurs at higher temperatures. Product ions also appear at m/z = 50, 51, 52, and 53. At each of these masses, the ions $C_4H_n^+$ are nominally isobaric with the $C_3H_{n-2}N^+$ ions for $n = 2-5$. Thermochemical calculations[56] suggest that all of the considered reaction pathways to form the observed product ions at these masses are exothermic. However, photoionization mass spectrometric experiments suggest that $m/z = 52$ is $C_4H_4^+$ formed by loss of HCN from ionized pyridine.[57] Further experiments using isotopically labeled substrates are necessary to determine the identity of these products.

Furan and Thiophene. Since the FA and SIFT results were similar for benzene, toluene, and pyridine, experimental results for Ar$^+$ with furan and the other VOCs were only obtained with the FA technique. The Ar$^+$ + furan reaction proceeds near the collision limit, and no significant temperature dependence was observed. The primary ionic product is $C_3H_3^+$ from the loss of HCO (or H + CO). The rate of reaction of Ar$^+$ with thiophene occurs near the ADO collision rate, and there is no appreciable temperature dependence. Nondissociative charge transfer only accounts for ~2% of the ionic products of the Ar$^+$ + thiophene reaction. Rich fragmentation chemistry is observed by the significant number of products, with the primary ionic products being $C_3H_3^+$, HCS$^+$, and $C_2H_2S^+$.

Cyclohexane, Cyclohexene, and Cyclooctene. The reactions of Ar$^+$ with the C_6H_{12}, C_6H_{10}, and C_8H_{14} hydrocarbons proceed at the collision rate and exhibit similar reaction pathways. For each of these reactions and at all of the temperatures considered, $C_3H_5^+$ is the primary product ion observed. Thermochemical calculations[56] show that the reaction channel to produce $C_3H_5^+$ is ≥40 kcal/mol more exothermic than the product channel that yields the next major ionic product, $C_3H_3^+$. Neither cyclohexane nor cyclooctene shows evidence of a nondissociative charge-transfer pathway; although in all cases, formation of the radical cation is exothermic. Significant dissociative charge transfer occurs in each of these reactions, yielding numerous products.

Tetrahydrofuran. The Ar$^+$ + tetrahydrofuran reaction proceeds by dissociative charge transfer. The primary ionic product, $C_3H_5^+$, is formed by charge transfer followed by loss of CH$_3$O (or CH$_2$=O + H). The fragment that appears at m/z = 43 could either be $C_3H_7^+$ or $C_2H_3O^+$. The reactions to yield either ionic product are both exothermic, -133 and -215 kcal/mol, respectively;[56] thus, further experiments are needed to characterize the exact nature of this product channel.

V. Discussion

It is interesting to consider the effect that multiple bonds within a C_6H_n ring has on the degree of fragmentation following charge transfer with Ar$^+$. When considering the loss of neutral C_nH_m from Ar$^+$ reactions with benzene, toluene, cyclohexene, and cyclohexane, the loss of C_3H_n is the primary process in the reactions of cyclohexene and cyclohexane with Ar$^+$. Loss of neutral C_2H_n fragments is the primary channel for the reaction of benzene with Ar$^+$; however, $C_6H_n^+$ ions are also present in substantial quantities. In the reaction of toluene with Ar$^+$, $C_7H_n^+$ are the primary ionic products. It appears that the presence of the CH$_3$ substituent minimizes significant fragmentation of the carbon skeleton in toluene following charge transfer with Ar$^+$. This effect might be accentuated with more or larger alkyl substituents, and this will be explored in the future.

TABLE 3: Rate Coefficients (k) and Branching Ratios (%) for Ar^{+} Reactions with Various Organic Compounds as a Function of Temperature[a]

reaction	SIFT (298 K) 0.5 Torr	FA (298 K) 0.5 Torr	FA (348 K) 0.5 Torr	FA (423 K) 1.0 Torr	FA (423 K) 0.5 Tor	ADO rate[a,b]
Ar^{+} + C_6H_6 →	$k = 1.59 \pm 0.10$	$k = 1.41 \pm 0.02$	$k = 1.95 \pm 0.21$	$k = 1.70 \pm 0.17$	$k = 2.84 \pm 0.38$	1.46
$C_3H_3^+ + C_3H_3 + Ar$	22	30	40	46	22	
$C_4H_2^+ + C_2H_2 + Ar$	6	6	4	3	7	
$C_4H_3^+ + C_2H_2 + H + Ar$	8	4	12	10	19	
$C_4H_4^+ + C_2H_2 + Ar$	40	39	27	25	21	
$C_4H_5^+ + C_2H + Ar$	3	3	2	1	2	
$C_5H_3^+ + CH_3 + Ar$	2	2	2	2	4	
$C_6H_4^+ + H_2 + Ar$	4	4	1	2	2	
$C_6H_5^+ + H + Ar$	11	6	5	4	7	
$C_6H_6^+ + Ar$	4	6	7	7	15	
Ar^{+} + toluene →	$k = 1.66 \pm 0.01$	$k = 1.66 \pm 0.12$	$k = 2.34 \pm 0.34$	$k = 2.16 \pm 0.29$	$k = 2.84 \pm 0.48$	1.63
$C_3H_3^+ + C_5H_5 + Ar$	14	7	23	29	11	
$C_4H_3^+ + C_3H_5 + Ar$	10	6	6	6	13	
$C_4H_5^+ + C_3H_3 + Ar$	8	4	2	3	6	
$C_5H_5^+ + C_2H_3 + Ar$	8	12	17	13	21	
$C_5H_6^+ + C_2H_2 + Ar$	7	3	3	2	3	
$C_6H_5^+ + CH_3 + Ar$	7					
$C_7H_6^+ + H_2 + Ar$	4					
$C_7H_7^+ + H + Ar$	35	59	37	38	31	
$C_7H_8^+ + Ar$	7	9	12	10	15	
Ar^{+} + pyridine →	$k = 2.29 \pm 0.18$	$k = 1.92 \pm 0.10$	$k = 2.23 \pm 0.09$	$k = 1.78 \pm 0.16$		2.13
$C_3H_3^+ + C_2H_2N + Ar$	12	21	26	32		
$C_4H_2^+ + CH_3N + Ar$ or $C_3N^+ + C_2H_5 + Ar$	7	2	5	6		
$C_4H_3^+ + CH_2N + Ar$ or $C_3HN^+ + C_2H_4 + Ar$	4	9	18	8		
$C_4H_4^+ + CHN + Ar$ or $C_3H_2N^+ + C_2H_3 + Ar$	56	53	36	40		
$C_4H_5^+ + CN + Ar$ or $C_3H_3N^+ + C_2H_2 + Ar$	10	7	6	6		
$C_5H_4N^+ + H + Ar$	9	5	3	6		
$C_5H_5N^+ + Ar$	2	4	5	3		
Ar^{+} + furan →		$k = 1.10 \pm 0.03$	$k = 1.41 \pm 0.11$	$k = 1.28 \pm 0.05$		1.55
$C_3H_2^+ + CH_2O + Ar$		8	11	13		
$C_3H_3^+ + HCO + Ar$		86	83	83		
$C_2H_2O^+ + C_2H_2 + Ar$		4	4	3		
$C_4H_4O^+ + Ar$		2	2			
Ar^{+} + thiophene →	$k = 1.50 \pm 0.05$	$k = 1.27 \pm 0.09$	$k = 1.71 \pm 0.10$	$k = 1.31 \pm 0.09$		1.44
$C_3H_2^+ + CH_2S + Ar$	4	5	4	7		
$C_3H_3^+ + CS + H + Ar$	18	24	46	43		
$CHS^+ + C_3H_3 + Ar$	44	38	30	29		
$CH_3S^+ + C_3H + Ar$	3	3				
$C_4H_2^+ + H_2S + Ar$	3	1				
$C_4H_3^+ + HS + Ar$	4	4	2	3		
$C_4H_4^+ + S + Ar$	4	1				
$C_2HS^+ + C_2H_3 + Ar$	4	1	3	3		
$C_2H_2S^+ + C_2H_2 + Ar$	12	16	12	12		
$C_3HS^+ + CH_3 + Ar$	2	3				
$C_4H_3S^+ + H + Ar$	2	2				
$C_4H_4S^+ + Ar$	2	2	3	2		
Ar^{+} + cyclohexene →	$k = 1.40 \pm 0.05$	$k = 1.28 \pm 0.06$	$k = 1.58 \pm 0.14$	$k = 1.18 \pm 0.04$	$k = 2.08 \pm 0.19$	1.44
$C_3H_3^+ + C_3H_7 + Ar$	24	27	37	42	24	
$C_3H_5^+ + C_3H_5 + Ar$	41	32	42	40	34	
$C_3H_6^+ + C_3H_4 + Ar$	4	4	3	3	3	
$C_4H_5^+ + C_2H_5 + Ar$	6	9	6	5	9	
$C_4H_6^+ + C_2H_4 + Ar$	7	17	8	8	16	
$C_4H_7^+ + C_2H_3 + Ar$	4	4	2	3	6	
$C_5H_7^+ + CH_3 + Ar$	3	7	2		5	
$C_6H_{10}^+ + Ar$	1				3	
Ar^{+} + cyclooctene →	$k = 1.44 \pm 0.01$	$k = 1.37 \pm 0.08$	$k = 1.81 \pm 0.13$	$k = 1.42 \pm 0.02$	$k = 2.45 \pm 0.22$	2.00
$C_3H_3^+ + C_5H_{11} + Ar$	10	9	17	44	10	
$C_3H_5^+ + C_5H_9 + Ar$	44	40	51	3	37	
$C_3H_6^+ + C_5H_8 + Ar$	5	3	4	2	3	
$C_3H_7^+ + C_5H_7 + Ar$	6		3	6	3	
$C_4H_5^+ + C_4H_9 + Ar$	5	5	4	13	8	
$C_4H_6^+ + C_4H_8 + Ar$	13	18	12	6	16	
$C_4H_7^+ + C_4H_7 + Ar$	5	7	3	8	10	
$C_5H_7^+ + C_3H_7 + Ar$	11	14	7		10	
$C_5H_8^+ + C_3H_6 + Ar$		3				
$C_6H_{10}^+ + C_2H_4 + Ar$					4	

Reactions of Ar$^+$ with Volatile Organic Compounds

J. Phys. Chem. A, Vol. 104, No. 48, 2000 **11325**

TABLE 3. (Continued)

reaction	SIFT (298 K) 0.5 Torr	FA (298 K) 0.5 Torr	FA (348 K) 0.5 Torr	FA (423 K) 1.0 Torr	FA (423 K) 0.5 Tor	ADO rate^{a,b}
Ar$^+$ + cyclohexane →	$k = 1.51 \pm 0.11$	$k = 1.00 \pm 0.06$	$k = 1.38 \pm 0.02$	$k = 1.31 \pm 0.08$		1.49
C$_3$H$_3^+$ + C$_3$H$_8$ + H + Ar	8	16	12	18		
C$_3$H$_5^+$ + C$_3$H$_7$ + Ar	60	54	68	63		
C$_3$H$_6^+$ + C$_3$H$_6$ + Ar	8	9	10	10		
C$_3$H$_7^+$ + C$_3$H$_5$ + Ar	8	4	2			
C$_4$H$_6^+$ + C$_2$H$_6$ + Ar	3	2	2			
C$_4$H$_7^+$ + C$_2$H$_5$ + Ar	9	10	4	9		
C$_4$H$_8^+$ + C$_2$H$_4$ + Ar	4	5	2			
Ar$^+$ + tetrahydrofuran →	$k = 1.75 \pm 0.09$	$k = 1.19 \pm 0.19$	$k = 1.70 \pm 0.04$	$k = 1.35 \pm 0.07$		2.07
C$_3$H$_3^+$ + CH$_4$ + OH + Ar	11	7	17	22		
C$_3$H$_5^+$ + CH$_3$O + Ar	68	59	59	63		
C$_3$H$_6^+$ + CH$_2$O + Ar	7	15	15	10		
C$_2$H$_3$O$^+$ + C$_2$H$_5$O + Ar or C$_3$H$_7^+$ + HCO + Ar	11	12	7	6		
C$_4$H$_5$O$^+$ + H + H$_2$ + Ar	1	3	1			
C$_4$H$_7$O$^+$ + H + Ar	2	3	1			

^{a} The rate coefficients are in units of 10^{-9} cm^3/s. ^{b} The ADO rate coefficients are calculated using the experimental dipole moment and polarizability (obtained from *The Handbook of Chemistry and Physics*, 71st ed.; CRC Press: Boca Raton, FL, 1990−91) for all compounds, except furan and cyclooctene (which are derived from B3LYP/6-31G* vibrational frequency analyses).

TABLE 4: Rate Coefficients (k) and Branching Ratios (%) for Ar$^+$ Reactions with Benzene, Toluene, and Pyridine Studied with the SIFT Technique at 0.7 Torr and as a Function of Temperature^a

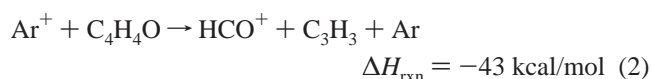| reaction	298 K (0.5 Torr)	298 K (0.7 Torr)	423 K (0.7 Torr)
Ar$^+$ + C$_6$H$_6$ →	$k = 1.59 \pm 0.10$	$k = 1.47 \pm 0.03$	$k = 1.61 \pm 0.17$
C$_3$H$_3^+$ + C$_3$H$_3$ + Ar	22	16	20
C$_4$H$_2^+$ + C$_2$H$_2$ + Ar	6	14	13
C$_4$H$_3^+$ + C$_2$H$_2$ + H + Ar	8	12	22
C$_4$H$_4^+$ + C$_2$H$_2$ + Ar	40	25	20
C$_4$H$_5^+$ + C$_2$H + Ar	3	7	5
C$_5$H$_3^+$ + CH$_3$ + Ar	2	3	6
C$_6$H$_4^+$ + H$_2$ + Ar	4	7	3
C$_6$H$_5^+$ + H + Ar	11	10	10
C$_6$H$_6^+$ + Ar	4	6	3
Ar$^+$ + toluene →	$k = 1.66 \pm 0.01$	$k = 1.32 \pm 0.20$	$k = 1.70 \pm 0.16$
C$_3$H$_3^+$ + C$_5$H$_5$ + Ar	14	16	45
C$_4$H$_3^+$ + C$_3$H$_5$ + Ar	10	6	15
C$_4$H$_5^+$ + C$_3$H$_3$ + Ar	8	5	5
C$_5$H$_5^+$ + C$_2$H$_3$ + Ar	8	3	7
C$_5$H$_6^+$ + C$_2$H$_2$ + Ar	7	3	2
C$_6$H$_5^+$ + CH$_3$ + Ar	7	0	4
C$_6$H$_5$CH$^+$ + H$_2$ + Ar	4	2	3
C$_6$H$_5$CH$_2^+$ + H + Ar	35	59	17
C$_6$H$_5$CH$_3^+$ + Ar	7	6	2
Ar$^+$ + pyridine →	$k = 2.41 \pm 0.22$	$k = 2.01 \pm 0.14$	$k = 2.07 \pm 0.24$
C$_3$H$_3^+$ + C$_2$H$_2$N + Ar	11	12	9
C$_4$H$_2^+$ or C$_3$N$^+$	7	9	26
C$_4$H$_3^+$ or C$_3$HN$^+$	4	8	15
C$_4$H$_4^+$ or C$_3$H$_2$N$^+$	56	52	36
C$_4$H$_5^+$ or C$_3$H$_3$N$^+$	10	9	7
C$_5$H$_4$N$^+$ + H + Ar	9	8	4
C$_5$H$_5$N$^+$ + Ar	2	3	3

^{a} The rate coefficients are in units of 10^{-9} cm^3/s.

Similar behavior is not observed when considering the reaction products of furan and tetrahydrofuran. Loss of neutral CH$_m$O, or the appearance of C$_3$H$_n^+$, is the primary process occurring when each of these ions undergo reaction with Ar$^+$. For furan, loss of neutral HCO (or CO + H) is dominant, but for THF, loss of CH$_3$O (or CH$_2$=O + H) is the major process. The reaction of Ar$^+$ with thiophene exhibits a richer chemistry than either furan or tetrahydrofuran. Interestingly, the primary product channel in the thiophene reaction with Ar$^+$ is the loss of C$_3$H$_3$ to yield HCS$^+$, and fragmentation pathways to generate C$_2$H$_2$ or CS are the next most favorable processes. Upon comparison of the reaction pathways for thiophene and furan, many of these reaction pathways for furan with Ar$^+$ are exothermic but are not observed. For example, the most

prominent reaction pathway (44%) for Ar$^+$ with thiophene at 298 K is

$$Ar^+ + C_4H_4S \rightarrow HCS^+ + C_3H_3 + Ar$$
$$\Delta H_{rxn} = -66 \text{ kcal/mol} \quad (1)$$
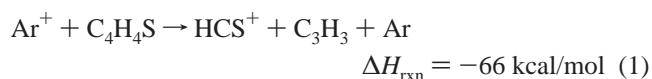
The corresponding reaction for Ar$^+$ with furan is

$$Ar^+ + C_4H_4O \rightarrow HCO^+ + C_3H_3 + Ar$$
$$\Delta H_{rxn} = -43 \text{ kcal/mol} \quad (2)$$

but is not observed at all. Instead C$_3$H$_3^+$ and HCO (or CO + H) is observed as the dominant product channel, although this
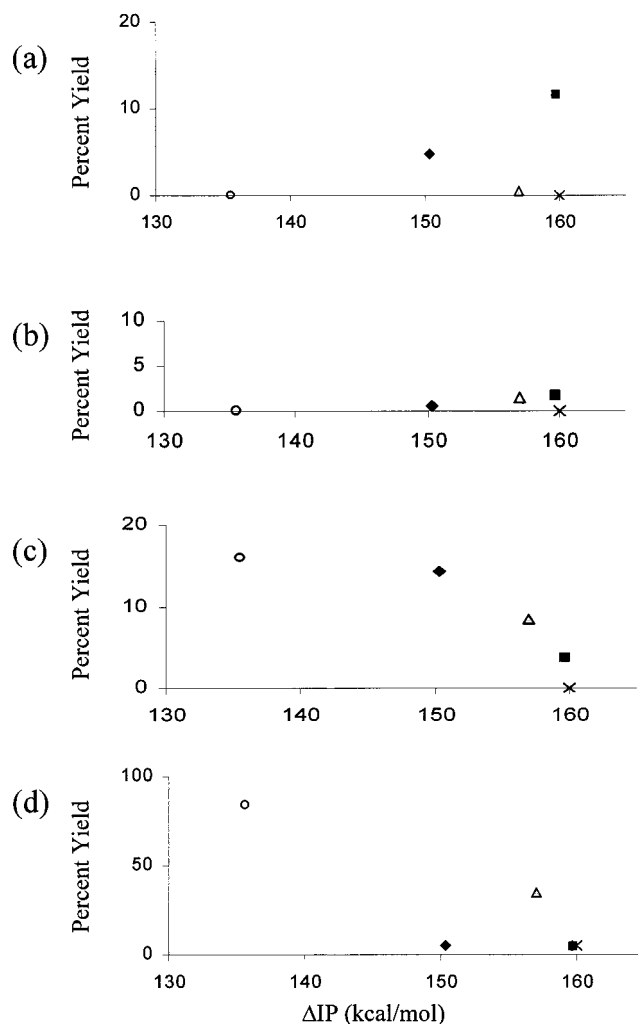
Figure 4. Branching ratios, normalized to the degree of unsaturation, as a function of ΔIP for benzene (diamond), toluene (square), cyclohexene (triangle), cyclohexane (circle), and cyclooctene (x): (a) loss of zero heavy atoms, (b) loss of 1 heavy atom, (c) loss of 2 heavy atoms, and (d) loss of 3 heavy atoms.

reaction channel is only 3 kcal/mol more favorable thermodynamically.

The ionization potentials (IP) of the neutral compounds used in this study range from 203.4 to 227.8 kcal/mol, and the IP of Ar is 363.4 kcal/mol. In Figure 4, the branching ratios are plotted for the loss of the number of neutral heavy atoms as a function of the ΔIP, where $\Delta IP = IP_{Ar} - IP_{VOC}$. The neutral heavy atom loss (along with some number of H atoms) has been normalized to the degree of unsaturation of the neutral VOC, and the results are plotted for the reactions of Ar^+ with benzene, toluene, cyclohexene, cyclooctene, and cyclohexane. While there is a substantial amount of scatter in the plots, the general trends suggest that the loss of zero heavy atoms and a single heavy atom increases as the ΔIP increases. The opposite trend is observed for the loss of 2 and 3 heavy atoms; that is, as the ΔIP increases between Ar and the neutral species, fewer neutral fragments containing 2 and 3 heavy atoms are lost following charge transfer. It would be interesting to consider these reactions over a broader range of ΔIP energies, and such efforts are in progress.

VI. Conclusions

The reactions of atmospheric positive ions with a variety of organic compounds have been studied using a new VTFA

complemented with a SIFT, which utilizes a quadrupole deflector. Calibration reactions of N_2^+ and CO_2^+ with small volatile molecules suggest that accurate reaction rate coefficients can be obtained using both the FA and FA-SIFT techniques.

The dissociative charge-transfer reactions of Ar^+ with a series of volatile organic compounds (benzene, toluene, pyridine, furan, thiophene, cyclohexene, cyclooctene, cyclohexane, and tetrahydrofuran) have been studied as a function of temperature. Very little temperature dependence was observed for the rate coefficients from 298 to 423 K. Significant fragmentation does occur following charge transfer, and the degree of fragmentation appears to be somewhat correlated to the difference in IP between Ar^+ and the neutral organic reactant. Some trends in the product branching ratios are observed when plotted as a function of ΔIP.

Future work will include studying similar reactions as a function of temperature with other ionized constituents of air, such as NO^+, O_2^+, CO_2^+, O^+, and N^+. It will be interesting to determine how product distributions change as a function of total energy. The IP of Ar^+ is quite high (363.4 kcal/mol), while those of the aforementioned ions are 213.3, 278.1, 317.5, 314.1, and 335.1 kcal/mol, respectively. It will be of further interest to determine how the chemistry changes with N_2^+ which has a similar IP (359.3 kcal/mol) as Ar.

References and Notes

(1) Midey, A. J.; Viggiano, A. A. *J. Chem. Phys.* **1998**, *109*, 5257−5263.

(2) Dotan, I.; Midey, A. J.; Viggiano, A. A. *J. Am. Soc. Mass Spectrom.* **1999**, *10*, 815−820.

(3) Ehbrecht, A.; Mustafa, N.; Ottinger, C.; Herman, Z. *J. Chem. Phys.* **1996**, *105*, 9833−9846.

(4) Chiu, Y.-H.; Dressler, R. A.; Levandier, D. J.; Williams, S.; Murad, E. *J. Chem. Phys.* **1999**, *110*, 4291−4299.

(5) Rincon, M. E.; Pearson, J.; Bowers, M. T. *J. Phys. Chem.* **1988**, *92*, 4290−4294.

(6) Fairley, D. A.; Milligan, D. B.; Freeman, C. G.; McEwan, M. J.; Spanel, P.; Smith, D. *Int. J. Mass Spectrom.* **1999**, *193*, 35−43.

(7) Ferguson, E. E.; Fehsenfeld, F. C.; Schmeltekopf, A. L. *Adv. At. Mol. Phys.* **1969**, *5*, 1−56.

(8) Adams, N. G.; Smith, D. *Int. J. Mass Spectrom. Ion Phys.* **1976**, *21*, 349−359.

(9) Smith, D.; Adams, N. G. *Adv. Gas-Phase Mol. Phys.* **1988**, *24*, 1−49.

(10) Dupeyrat, G.; Rowe, B. R.; Fahey, D. W.; Albritton, D. L. *Int. J. Mass Spectrom. Ion Phys.* **1982**, *44*, 1−18.

(11) Doren, J. M. V.; Barlow, S. E.; DePuy, C. H.; Bierbaum, V. M. *Int. J. Mass Spectrom. Ion Proc.* **1987**, *81*, 85−100.

(12) Mackay, G. I.; Vlachos, G. D.; Bohme, D. K.; Schiff, H. I. *Int. J. Mass Spectrom. Ion Phys.* **1980**, *36*, 259−70.

(13) Baranov, V.; Bohme, D. K. *Int. J. Mass Spectrom. Ion Proc.* **1996**, *154*, 71−88.

(14) Fishman, V. N.; Grabowski, J. J. *Int. J. Mass Spectrom. Ion Proc.* **1998**, *177*, 175−186.

(15) Kato, S.; Frost, M. J.; Bierbaum, V. M.; Leone, S. R. *Rev. Sci. Instrum.* **1993**, *64*, 2808−2820.

(16) Marinelli, P. J.; Paulino, J. A.; Sunderlin, L. S.; Wenthold, P. G.; Poutsma, J. C.; Squires, R. R. *Int. J. Mass Spectrom. Ion Proc.* **1994**, *130*, 89−105.

(17) Viggiano, A. A.; Morris, R. A.; Dale, F.; Paulson, J. F.; Giles, K.; Smith, D.; Su, T. *J. Chem. Phys.* **1990**, *93*, 1149−1157.

(18) Iraqi, M.; Petrank, A.; Peres, M.; Lifshitz, C. *Int. J. Mass Spectrom. Ion Proc.* **1990**, *100*, 679.

(19) Squires, R. R. *Int. J. Mass Spectrom. Ion Proc.* **1992**, *118/119*, 263−358.

(20) Graul, S. T.; Squires, R. R. *Mass Spectrom. Rev.* **1988**, *7*, 263−358.

(21) Barckholtz, C. Ph.D. Thesis, The Ohio State University, 1998.

(22) Zeman, H. D. *Rev. Sci. Instrum.* **1977**, *48*, 1079−1085.

(23) Farley, J. W. *Rev. Sci. Instrum.* **1985**, *56*, 1834−1835.

Reactions of Ar⁺ with Volatile Organic Compounds

J. Phys. Chem. A, Vol. 104, No. 48, 2000 **11327**

(24) DeTuri, V. F.; Hintz, P. A.; Ervin, K. M. *J. Phys. Chem. A* **1997**, *101*, 5969−86.

(25) Plastridge, B.; Cohen, M. H.; Cowen, K. A.; Wood, D. A.; Coe, J. V. *J. Phys. Chem.* **1995**, *99*, 118−122.

(26) Mahaffy, P. R.; Lai, K. *J. Vac. Sci. Technol. A* **1990**, *8*, 3244−3246.

(27) Spence, T. G.; Burns, T. D.; Posey, L. A. *J. Phys. Chem. A* **1997**, *101*, 139−144.

(28) Arnold, S. T.; Viggiano, A. A.; Morris, R. A. *J. Phys. Chem. A* **1998**, *102*, 8881−8887.

(29) Midey, A. J.; Williams, S.; Arnold, S. T.; Dotan, I.; Morris, R. A.; Viggiano, A. A. *Int. J. Mass Spectrom.* **2000**, *195/96*, 327−339.

(30) Williams, S.; Midey, A. J.; Arnold, S. T.; Bench, P. M.; Viggiano, A. A.; Morris, R. A.; Maurice, L. Q.; Carter, C. D. *Progress on the Investigation of the Effects of Ionization on Hydrocarbon/Air Combustion Chemistry*; Ed.: Norfolk, VA, 1999; pp AIAA Paper 99-4907.

(31) Arnold, S. T.; Viggiano, A. A.; Morris, R. A. *J. Phys. Chem. A* **1997**, *101*, 9351−9358.

(32) Arnold, S. T.; Williams, S.; Dotan, I.; Midey, A. J.; Morris, R. A.; Viggiano, A. A. *J. Phys. Chem. A* **1999**, *103*, 8421−8432.

(33) Barckholtz, C.; Barckholtz, T. A.; Hadad, C. M. *J. Phys. Chem. A,* submitted.

(34) Fadden, M. J.; Hadad, C. M. *J. Phys. Chem. A* **2000**, *104*, 8121−8130.

(35) Fadden, M. J.; Hadad, C. M. *J. Phys. Chem. A* **2000**, *104*, 6324−6331.

(36) Fadden, M. J.; Hadad, C. M. *J. Phys. Chem. A* **2000**, *104*, 6088−6094.

(37) Fadden, M. J.; Barckholtz, C.; Hadad, C. M. *J. Phys. Chem. A* **2000**, *104*, 3004−3011.

(38) Barckholtz, C.; Fadden, M. J.; Hadad, C. M. *J. Phys. Chem. A* **1999**, *103*, 8108−8117.

(39) Barckholtz, C.; Barckholtz, T. A.; Hadad, C. M. *J. Am. Chem. Soc.* **1999**, *121*, 491−500.

(40) Frink, B. T. Ph.D. Thesis, The Ohio State University, 1999.

(41) Bond, J. J. M.S. Thesis, The Ohio State University, 1999.

(42) Sokolov, O. V.; Bond, J. J.; Geise, C. M.; Frink, B. T.; Cohen, M. H.; Hadad, C. M. Manuscript in preparation.

(43) Grabowski, J. J.; Zhang, L. *J. Am. Chem. Soc.* **1989**, *111*, 1193.

(44) Anicich, V. G. *J. Phys. Chem. Ref. Data* **1994**, *22*, 1469 and references therein.

(45) Dunkin, D. B.; Fehsenfeld, F. C.; Schmeltekopf, A. L.; Ferguson, E. E. *J. Chem. Phys.* **1968**, *49*, 1365.

(46) Kato, S.; Frost, M. J.; Bierbaum, V. M.; Leone, S. R. *Can. J. Chem.* **1994**, *72*, 625.

(47) Fite, W. L.; Rutherford, J. A.; Snow, W. R.; Lint, V. A. V. *Discuss. Faraday Soc.* **1962**, *33*, 264.

(48) Dotan, I.; Hierl, P. M.; Morris, R. A.; Viggiano, A. A. *Int. J. Mass Spectrom. Ion Proc.* **1997**, *167/168*, 223−230.

(49) McFarland, M.; Albritton, D. L.; Fehsenfeld, F. C.; Ferguson, E. E. *J. Chem. Phys.* **1973**, *59*, 6620.

(50) Lindinger, W.; McFarland, M.; Fehsenfeld, F. C.; Albritton, D. L.; Schmeltekopf, A. L.; Ferguson, E. E. *J. Chem. Phys.* **1975**, *63*, 2175.

(51) Miller, T. M.; Wetterskog, R. E.; Paulson, J. F. *J. Chem. Phys.* **1984**, *80*, 4922.

(52) Ikezoe, Y.; Matsuoka, S.; Takebe, M.; Viggiano, A. A. *Gas-Phase Ion−Molecule Reaction Rate Constants Through 1986*; Maruzen Company, Ltd.: Tokyo, 1987.

(53) Smith, D.; Adams, N. G.; Miller, T. M. *J. Chem. Phys.* **1978**, *69*, 308−318.

(54) Su, T.; Bowers, M. T. *Int. J. Mass Spectrom. Ion Phys.* **1973**, *12*, 347.

(55) Experiments were performed at 1 Torr by decreasing the pumping efficiency of the instrument.

(56) Lias, S. G.; Bartmess, J. E.; Liebman, J. F.; Holmes, J. L.; Levin, R. D.; Mallard, W. G. *J. Phys. Chem. Ref. Data* **1988**, *17*, 1.

(57) Eland, J. H. D.; Berkowitz, J. *Int. J. Mass Spectrom. Ion. Phys.* **1978**, *28*, 297−311.